



New Search for $\tau \rightarrow \mu\gamma$ and $\tau \rightarrow e\gamma$ Decays at Belle

Belle Collaboration

K. Hayasaka^w, K. Abe^{ar}, I. Adachi^h, H. Aihara^{at}, D. Anipko^a,
 K. Arinstein^a, V. Aulchenko^a, A. M. Bakich^{ap}, E. Barberio^v,
 A. Bay^s, I. Bedny^a, K. Belous^l, U. Bitenc^o, I. Bizjak^o,
 A. Bondar^a, A. Bozek^{ab}, M. Bračko^{h,u,o}, J. Brodzicka^{ab},
 M.-C. Chang^e, P. Chang^{aa}, Y. Chao^{aa}, A. Chen^y,
 W. T. Chen^y, B. G. Cheon^c, R. Chistovⁿ, Y. Choi^{ao},
 Y. K. Choi^{ao}, J. Dalseno^v, M. Danilovⁿ, M. Dash^{ay},
 A. Drutskoy^d, S. Eidelman^a, D. Epifanov^a, S. Fratina^o,
 N. Gabyshev^a, T. Gershon^h, A. Go^y, B. Golob^{t,o}, H. Ha^q,
 J. Haba^h, K. Hara^w, T. Hara^{ag}, H. Hayashii^x, M. Hazumi^h,
 D. Heffernan^{ag}, T. Hokuue^w, Y. Hoshi^{ar}, S. Hou^y,
 W.-S. Hou^{aa}, T. Iijima^w, K. Ikado^w, A. Imoto^x, K. Inami^w,
 A. Ishikawa^{at}, R. Itoh^h, M. Iwasaki^{at}, Y. Iwasaki^h, H. Kaji^w,
 J. H. Kang^{az}, H. Kawai^b, T. Kawasaki^{ad}, H. R. Khan^{au},
 H. Kichimi^h, S. K. Kim^{am}, Y. J. Kim^f, Y. Kozakai^w,
 P. Križan^{t,o}, P. Krokovny^h, R. Kulasiri^d, R. Kumar^{ah},
 C. C. Kuo^y, A. Kuzmin^a, Y.-J. Kwon^{az}, M. J. Lee^{am},
 S. E. Lee^{am}, T. Lesiak^{ab}, S.-W. Lin^{aa}, D. Liventsevⁿ,
 F. Mandl^m, T. Matsumoto^{av}, K. Miyabayashi^x, H. Miyake^{ag},
 H. Miyata^{ad}, Y. Miyazaki^w, G. R. Moloney^v, T. Mori^w,
 Y. Nagasakaⁱ, M. Nakao^h, H. Nakazawa^h, Z. Natkaniec^{ab},
 S. Nishida^h, O. Nitoh^{aw}, S. Ogawa^{aq}, T. Ohshima^w,
 S. Okuno^p, S. L. Olsen^g, Y. Onuki^{ak}, H. Ozaki^h, P. Pakhlovⁿ,
 G. Pakhlovaⁿ, H. Park^r, K. S. Park^{ao}, L. S. Peak^{ap},
 R. Pestotnik^o, L. E. Piilonen^{ay}, A. Poluektov^a, H. Sahoo^g,
 Y. Sakai^h, N. Satoyama^{an}, T. Schietinger^s, O. Schneider^s,

A. J. Schwartz^d, R. Seidl^{j,ak}, K. Senyo^w, M. E. Sevier^v,
M. Shapkin^ℓ, H. Shibuya^{aq}, B. Shwartz^a, J. B. Singh^{ah},
A. Sokolov^ℓ, A. Somov^d, N. Soni^{ah}, S. Stanič^{ae}, M. Starič^o,
H. Stoeck^{ap}, T. Sumiyoshi^{av}, F. Takasaki^h, K. Tamai^h,
N. Tamura^{ad}, M. Tanaka^h, G. N. Taylor^v, Y. Teramoto^{af},
X. C. Tian^{ai}, I. Tikhomirovⁿ, T. Tsuboyama^h, T. Tsukamoto^h,
S. Uehara^h, K. Ueno^{aa}, T. Uglovⁿ, S. Uno^h, P. Urquijo^v,
Y. Usov^a, G. Varner^g, S. Villa^s, A. Vinokurova^a,
C. C. Wang^{aa}, C. H. Wang^z, Y. Watanabe^{au}, E. Won^q,
Q. L. Xie^k, B. D. Yabsley^{ap}, A. Yamaguchi^{as}, Y. Yamashita^{ac},
M. Yamauchi^h, Z. P. Zhang^{al}, V. Zhilich^a, V. Zhulanov^a, and
A. Zupanc^o

^a*Budker Institute of Nuclear Physics, Novosibirsk, Russia*

^b*Chiba University, Chiba, Japan*

^c*Chonnam National University, Kwangju, South Korea*

^d*University of Cincinnati, Cincinnati, OH, USA*

^e*Department of Physics, Fu Jen Catholic University, Taipei, Taiwan*

^f*The Graduate University for Advanced Studies, Hayama, Japan*

^g*University of Hawaii, Honolulu, HI, USA*

^h*High Energy Accelerator Research Organization (KEK), Tsukuba, Japan*

ⁱ*Hiroshima Institute of Technology, Hiroshima, Japan*

^j*University of Illinois at Urbana-Champaign, Urbana, IL, USA*

^k*Institute of High Energy Physics, Chinese Academy of Sciences, Beijing, PR
China*

^ℓ*Institute for High Energy Physics, Protvino, Russia*

^m*Institute of High Energy Physics, Vienna, Austria*

ⁿ*Institute for Theoretical and Experimental Physics, Moscow, Russia*

^o*J. Stefan Institute, Ljubljana, Slovenia*

^p*Kanagawa University, Yokohama, Japan*

^q*Korea University, Seoul, South Korea*

^r*Kyungpook National University, Taegu, South Korea*

^s*Swiss Federal Institute of Technology of Lausanne, EPFL, Lausanne, Switzerland*

^t*University of Ljubljana, Ljubljana, Slovenia*

^u*University of Maribor, Maribor, Slovenia*

^v*University of Melbourne, Victoria, Australia*

^w*Nagoya University, Nagoya, Japan*

- ^x*Nara Women's University, Nara, Japan*
- ^y*National Central University, Chung-li, Taiwan*
- ^z*National United University, Miao Li, Taiwan*
- ^{aa}*Department of Physics, National Taiwan University, Taipei, Taiwan*
- ^{ab}*H. Niewodniczanski Institute of Nuclear Physics, Krakow, Poland*
- ^{ac}*Nippon Dental University, Niigata, Japan*
- ^{ad}*Niigata University, Niigata, Japan*
- ^{ae}*University of Nova Gorica, Nova Gorica, Slovenia*
- ^{af}*Osaka City University, Osaka, Japan*
- ^{ag}*Osaka University, Osaka, Japan*
- ^{ah}*Panjab University, Chandigarh, India*
- ^{ai}*Peking University, Beijing, PR China*
- ^{aj}*Princeton University, Princeton, NJ, USA*
- ^{ak}*RIKEN BNL Research Center, Brookhaven, NY, USA*
- ^{al}*University of Science and Technology of China, Hefei, PR China*
- ^{am}*Seoul National University, Seoul, South Korea*
- ^{an}*Shinshu University, Nagano, Japan*
- ^{ao}*Sungkyunkwan University, Suwon, South Korea*
- ^{ap}*University of Sydney, Sydney, NSW, Australia*
- ^{aq}*Toho University, Funabashi, Japan*
- ^{ar}*Tohoku Gakuin University, Tagajo, Japan*
- ^{as}*Tohoku University, Sendai, Japan*
- ^{at}*Department of Physics, University of Tokyo, Tokyo, Japan*
- ^{au}*Tokyo Institute of Technology, Tokyo, Japan*
- ^{av}*Tokyo Metropolitan University, Tokyo, Japan*
- ^{aw}*Tokyo University of Agriculture and Technology, Tokyo, Japan*
- ^{ay}*Virginia Polytechnic Institute and State University, Blacksburg, VA, USA*
- ^{az}*Yonsei University, Seoul, South Korea*

Abstract

We report on a search for the lepton flavor violating $\tau^- \rightarrow \mu^- \gamma$ and $\tau^- \rightarrow e^- \gamma$ decays based on 535 fb^{-1} of data accumulated at the Belle experiment. No signal is found and we set 90% confidence level upper limits on the branching ratios $\mathcal{B}(\tau^- \rightarrow \mu^- \gamma) < 4.5 \times 10^{-8}$ and $\mathcal{B}(\tau^- \rightarrow e^- \gamma) < 1.2 \times 10^{-7}$.

Key words: Decays of taus, lepton number, Taus

PACS: 13.35.Dx, 11.30.Fs, 14.60.Fg

1 Introduction

Lepton flavor violation (LFV) could appear in various new physics scenarios beyond the Standard Model, e.g., in the Minimal Supersymmetric extension (MSSM) [1], in Grand Unified Theories [2], and see-saw mechanisms [3]. In most models describing LFV in the τ lepton sector, the radiative decays $\tau \rightarrow \mu(e)\gamma$ have the largest probability; this has motivated many experimental searches [4–10]. Using 86 fb^{-1} of data recorded at the $\Upsilon(4S)$ resonance with the Belle experiment [11] at the KEKB asymmetric-energy e^+e^- collider [12] we have previously obtained the upper limits $\mathcal{B}(\tau^- \rightarrow \mu^- \gamma) < 3.1 \times 10^{-7}$ [13] and $\mathcal{B}(\tau^- \rightarrow e^- \gamma) < 3.9 \times 10^{-7}$ [14] at the 90% confidence level (CL). The BaBar collaboration subsequently obtained the upper limits $\mathcal{B}(\tau^- \rightarrow \mu^- \gamma) < 6.8 \times 10^{-8}$ [15] and $\mathcal{B}(\tau^- \rightarrow e^- \gamma) < 1.1 \times 10^{-7}$ [16] with 232.2 fb^{-1} of data. Here, we report on an updated analysis with 535 fb^{-1} of data, which corresponds to 4.77×10^8 produced $\tau^+\tau^-$ pairs [17].

The Belle detector is a large-solid-angle magnetic spectrometer that consists of a silicon vertex detector (SVD), a 50-layer central drift chamber (CDC), an array of aerogel threshold Cherenkov counters (ACC), a barrel-like arrangement of time-of-flight scintillation counters (TOF), and an electromagnetic calorimeter comprised of CsI(Tl) crystals (ECL) located inside a superconducting solenoid coil that provides a 1.5 T magnetic field. An iron flux-return located outside the coil is instrumented to detect K_L^0 mesons and to identify muons (KLM). The detector is described in detail elsewhere [11].

The basic analysis procedure is similar to our previous one [13,14]. The selection criteria for $\tau^- \rightarrow \mu^- \gamma/e^- \gamma$ are determined and optimized by examining Monte Carlo (MC) simulated signal and background (BG) events, including generic $\tau^+\tau^-$, $q\bar{q}$ ($q = u, d, s, c, b$), Bhabha, $\mu^+\mu^-$, and two-photon events. The BG $\tau^+\tau^-$ events are generated by the KKMC/TAUOLA [17] and the response of the Belle detector is simulated by the GEANT3 [18] based program.

Photon candidates are selected from ECL clusters that are consistent with an electromagnetic shower shape and not associated with charged tracks. Muon candidates are identified by using a muon likelihood ratio, \mathcal{L}_μ [19], which is based on the difference between the range of the track calculated from the particle momentum and that measured by the KLM. This ratio includes the value of χ^2 formed from the KLM hit locations with respect to the extrapolated track. The muon identification efficiency for these selection criteria ($\mathcal{L}_\mu > 0.95$) is 90%, with a pion fake probability of 0.8%. Identification of electrons uses an electron likelihood ratio, \mathcal{L}_e , based on dE/dx information from the CDC, the ratio of the energy deposited in the ECL to the momentum measured by the CDC and SVD, the shower shape in the ECL, hit information from the ACC and matching between the positions of the charged track and the ECL

cluster [20]. The electron identification efficiency for these selection criteria ($\mathcal{L}_e > 0.9$) is 95%, with a pion fake probability of 0.07%.

2 $\tau \rightarrow \mu\gamma$

2.1 Event Selection

We select events that include exactly two oppositely charged tracks and at least one photon, consistent with $\tau^+\tau^-$ decays: one τ^\pm (signal side) decays to $\mu^\pm\gamma$ and the other (tag side) decays to a charged particle that is not a muon (denoted hereafter as $\not{\mu}$), neutrino(s) and any number of photons. In this analysis, before particle identification, we assign the pion mass to all charged tracks to calculate their energies and momenta in the center-of-mass (CM) frame.

Each track must have a momentum $p^{\text{CM}} < 4.5$ GeV/ c in the CM frame to reduce contamination from Bhabha and $\mu^+\mu^-$ events and a transverse component to the beam axis of $p_t > 0.1$ GeV/ c within the detector fiducial region, $-0.866 < \cos\theta < 0.956$, to suppress two-photon background. Here θ is the polar angle with respect to the z axis, which is anti-parallel to the e^+ beam. (Hereafter, all the variables defined in the CM frame have superscripts “CM”.) Each photon is required to have an energy $E_\gamma > 0.1$ GeV within the fiducial region. The total energy in the CM frame must be $E_{\text{total}}^{\text{CM}} < 10.5$ GeV to further suppress Bhabha and $\mu^+\mu^-$ events. The magnitude of the thrust vector, constructed from all selected charged tracks and photons mentioned above, is required to be in the range from 0.90 to 0.98 in order to suppress $\mu^+\mu^-$ and $q\bar{q}$ background (Fig. 1(a)).

For muon identification, we require a likelihood ratio of $\mathcal{L}_\mu > 0.95$ and $p > 1.0$ GeV/ c . On the tag side, a track with $\mathcal{L}_\mu < 0.8$ is defined as $\not{\mu}$. The photon that forms a $(\mu\gamma)$ candidate is required to have $E_\gamma > 0.5$ GeV and $-0.602 < \cos\theta_\gamma < 0.829$ to remove any spurious combinations of γ 's.

The opening angle between the μ and γ of the $(\mu\gamma)$ candidate, $0.4 < \cos\theta_{\mu\gamma}^{\text{CM}} < 0.8$, is useful in rejecting $\tau^+\tau^-$ background that contains π^0 's from τ decays (Fig. 1(b)). The sum of the energies of the two charged tracks and the photon of the $(\mu\gamma)$ candidate, $E_{\text{sum}}^{\text{CM}}$, should be less than 9.0 GeV to reject $\mu^+\mu^-$ events. The opening angle between the two tracks should be greater than 90° in the CM frame, and the opening angle between the μ and the boost direction of its mother τ from the CM frame is required to satisfy $\cos\theta_{\mu\tau} < 0.4$ in the τ rest frame, to remove combinations of μ 's and γ 's from BG (Fig. 1(c)).

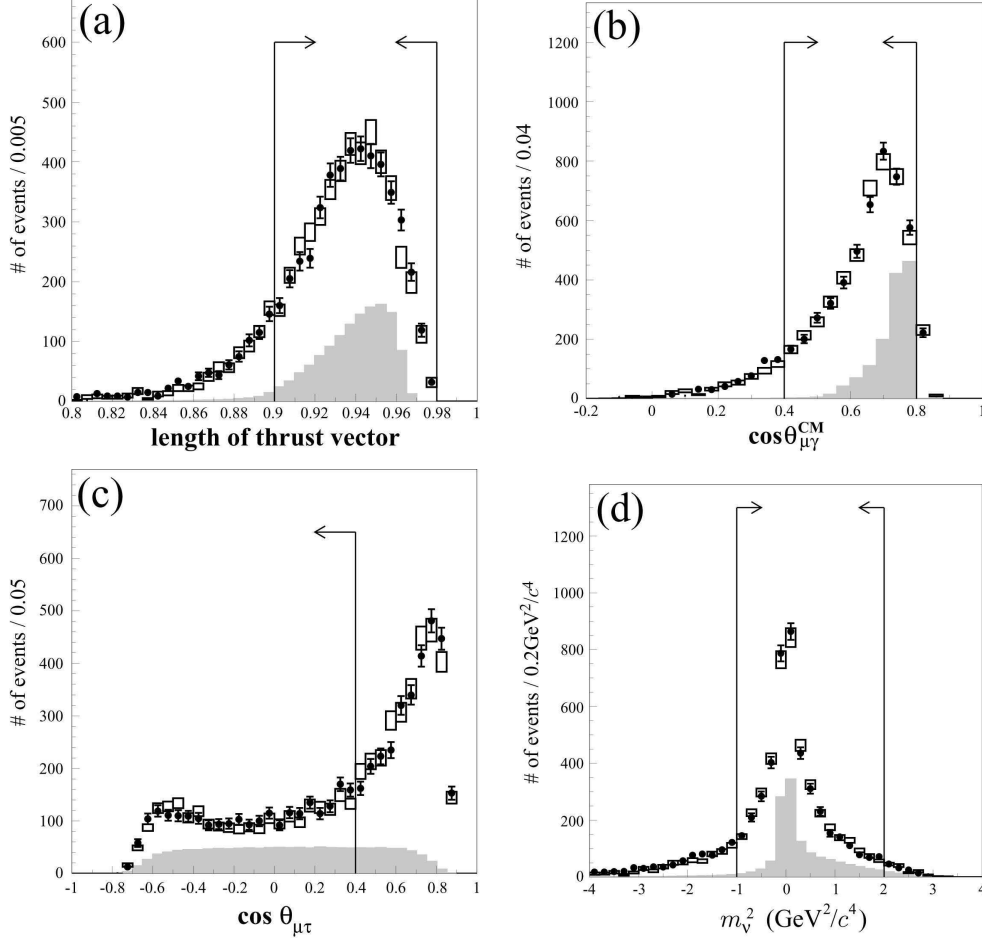


Fig. 1. (a) Magnitude of the thrust vector, (b) $\cos \theta_{\mu\gamma}^{\text{CM}}$, (c) $\cos \theta_{\mu\tau}$ and (d) m_ν^2 distributions for $\tau \rightarrow \mu\gamma$. Dots are data, open boxes show the BG MC distribution and shaded histograms are the signal MC. Arrows indicate the selected region. Here, the branching ratio of $\tau \rightarrow \mu\gamma$ is assumed to be 1.0×10^{-5} for the signal MC histograms. The requirements on particle identification for the signal and tag sides and $1.5 \text{ GeV}/c^2 < M_{\text{inv}} < 2.0 \text{ GeV}/c^2$, $-0.5 \text{ GeV} < \Delta E < 0.5 \text{ GeV}$ are imposed here.

The following constraints on the momentum and the polar angle of the missing particle are imposed: $p_{\text{miss}} > 0.4 \text{ GeV}/c$ and $-0.866 < \cos \theta_{\text{miss}} < 0.956$. Here, p_{miss} is calculated by subtracting the sum of the momenta of all charged tracks and photons from the beam momenta. To remove the $\tau^+\tau^-$ background events, a requirement on the opening angle between the tag-side track and the missing particle is applied, $0.4 < \cos \theta_{\text{miss}-\mu}^{\text{CM}} < 0.98$. We calculate the missing mass squared on the tag side, $m_\nu^2 = (E_{\mu\gamma}^{\text{CM}} - E_{\text{tag}}^{\text{CM}})^2 - (p_{\text{miss}}^{\text{CM}})^2$, where $E_{\mu\gamma}^{\text{CM}}$ ($E_{\text{tag}}^{\text{CM}}$) is the sum of the energy of the signal side μ and γ in the CM frame, and then require $-1.0 \text{ GeV}^2/c^4 < m_\nu^2 < 2.0 \text{ GeV}^2/c^4$, as shown in Fig. 1(d). Finally, the condition, $p_{\text{miss}} > -5 \times m_{\text{miss}}^2 - 1$ and $p_{\text{miss}} > 1.5 \times m_{\text{miss}}^2 - 1$, is imposed. The missing mass is given by $m_{\text{miss}}^2 = E_{\text{miss}}^2 - p_{\text{miss}}^2$ (in GeV/c^2), where E_{miss} is the sum of the beam energies minus the visible energy. This relation is illustrated

by Fig. 2.

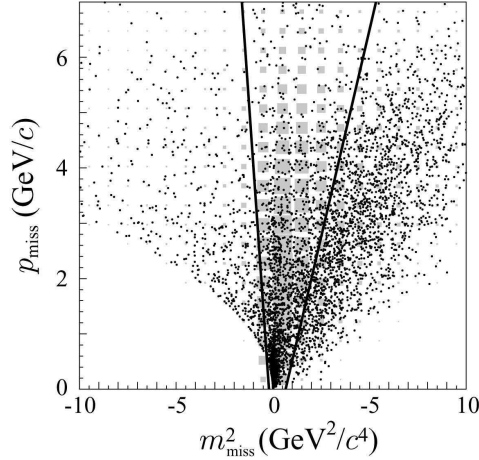


Fig. 2. Distributions in $m_{\text{miss}}^2 - p_{\text{miss}}$ plane for data (dot) and signal MC (shaded box) events. Events are chosen between the two lines in the figure. Also, $p_{\text{miss}} > 0.4$ is required. The two lines correspond to the equations $p_{\text{miss}} = -5 \times m_{\text{miss}}^2 - 1$ and $p_{\text{miss}} = 1.5 \times m_{\text{miss}}^2 - 1$. The applied requirements are the same as those in Fig. 1.

2.2 Background contribution

After the selection requirements described in the previous subsection, the dominant BG source is $\tau^+\tau^-$ events with the decay $\tau^\pm \rightarrow \mu^\pm\nu_\mu\nu_\tau$ or $\tau^\pm \rightarrow \pi^\pm\nu_\tau$ where the π is misidentified as a μ and is then combined with a photon from initial state radiation or beam BG. Another source is the radiative $e^+e^- \rightarrow \mu^+\mu^-$ process.

Two variables are used to identify the signal: M_{inv} , the invariant mass of $(\mu\gamma)$, and $\Delta E = E_{\mu\gamma}^{\text{CM}} - E_{\text{beam}}^{\text{CM}}$, the energy difference between the $(\mu\gamma)$ energy and the beam energy in the CM frame, where the signal should have $M_{\text{inv}} \sim m_\tau$ and $\Delta E \sim 0$. The resolutions in M_{inv} and ΔE are estimated by fitting asymmetric Gaussians to the signal MC distributions giving $\sigma_{M_{\text{inv}}}^{\text{high/low}} = 14.49 \pm 0.10 / 24.24 \pm 0.13$ MeV/ c^2 and $\sigma_{\Delta E}^{\text{high/low}} = 35.29 \pm 0.49 / 81.41 \pm 0.94$ MeV, where $\sigma^{\text{high/low}}$ means the standard deviation on the higher/lower side of the peak.

To compare the data and MC simulation, we examine a 5σ region with $1.65 \text{ GeV}/c^2 < M_{\text{inv}} < 1.85 \text{ GeV}/c^2$ and $-0.41 \text{ GeV} < \Delta E < 0.17 \text{ GeV}$, as shown in Fig. 3(a). A ‘blind analysis’ method is used: a 3σ region as indicated by the dashed ellipse in Fig. 3(a) is ‘blinded’ (not examined) until all selection criteria are finalized. The detection efficiency for this region is determined from MC simulation to be 6.05%.

After the selections, we find 71 events remaining in data and 73.4 ± 6.7 events

in MC in the 5σ region outside the blinded ellipse. According to MC, the remaining events are dominated by the initial state radiation process $\tau^+\tau^-\gamma$ – 58.8 ± 4.3 (70.3 ± 4.7) events and also include 13.1 ± 4.9 (15.0 ± 5.3) $\mu^+\mu^-\gamma$ events with incorrect μ identification, and 1.6 ± 1.6 (3.2 ± 2.2) two-photon events, where the numbers in parentheses are the BGs that remain in the entire 5σ region.

This background composition was understood in the previous analysis; the $\tau^+\tau^-\gamma$ process yields contributions in the $\Delta E < 0$ region, while $\mu^+\mu^-\gamma$ events mostly have $\Delta E > 0$. This BG distribution is well represented by a combination of Landau and Gaussian functions, as found in Ref. [14]. To obtain the final BG distribution, we perform a binned maximum likelihood fit to the candidates in the 5σ region outside the blinded ellipse. The final event distribution in the data is very similar to that obtained from the MC: $(79.0 \pm 9.2)\%$ is $\tau^+\tau^-\gamma$, $(15.8 \pm 8.5)\%$ is $\mu^+\mu^-\gamma$, and $(5.2 \pm 4.1)\%$ is from $e^+e^-\gamma \rightarrow e^+e^-\mu^+\mu^-$.

2.3 Signal extraction

After unblinding, we find 23 and 94 data events in the blinded and 5σ regions, respectively, while 15.0 ± 3.1 and 88.4 ± 7.4 events are expected from the MC. Figure 3(a) shows the final event distributions (data and signal MC) in the $M_{\text{inv}}-\Delta E$ plane.

In order to extract the number of signal events, we employ an unbinned extended maximum likelihood (UEML) fit with the following likelihood function:

$$\mathcal{L} = \frac{e^{-(s+b)}}{N!} \prod_{i=1}^N (sS_i + bB_i). \quad (1)$$

Here, N is the number of observed events; s and b are the numbers of signal and BG events to be extracted, respectively; S_i and B_i are the signal and BG probability density functions (PDF), where i indicates the i -th event; the shape of the signal PDF, S_i , is obtained by smoothing the signal MC distribution, and B_i is the PDF for the background mentioned above, whose distribution is concentrated around $\Delta E \simeq -0.2$ GeV, as indicated by the solid line in Fig. 3(a). To enhance the signal detection sensitivity and to avoid this dense BG region, we use a 2σ ellipse as the signal region for the UEML fit. The result of the fit is $s = -3.9_{-3.2}^{+3.6}$, $b = 13.9_{-4.8}^{+6.0}$ with $N = 10$.

Figure 3(b) shows the event distribution within the 2σ band of the shorter ellipse axis, projected onto the longer ellipse axis, and the best fit curve. No events are found near the peak of the signal distribution. The negative s value is consistent with no signal.

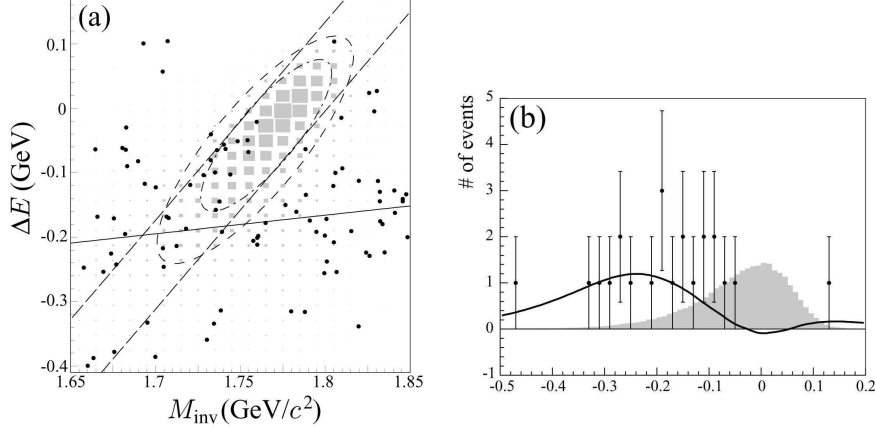


Fig. 3. (a) $M_{\text{inv}} - \Delta E$ distribution in the search for $\tau \rightarrow \mu\gamma$ in the 5σ region. Dots are the data and shaded boxes indicate the signal MC. The dashed ellipse shows the 3σ blinded region and the dot-dashed ellipse is the 2σ signal region. The dashed lines indicate the 2σ band of the shorter ellipse axis, projected onto the longer ellipse axis. The solid line indicates the dense BG region. (b) Data distribution within the 2σ band. Here, $\mathcal{E} \equiv \Delta E - \Delta E^{(0)}$, $\mathcal{M} \equiv 3.0 \times c^2 \times (M_{\text{inv}} - M_{\text{inv}}^{(0)})$ and $\alpha = 46^\circ$. We obtain the most probable values $\Delta E^{(0)}$ and $M_{\text{inv}}^{(0)}$, $M_{\text{inv}}^{(0)} = 1.776 \text{ GeV}/c^2$, $\Delta E^{(0)} = -5 \text{ MeV}$, by fitting the signal MC distribution to an asymmetric Gaussian. Points with error bars are the data and the shaded histogram is the signal MC assuming a branching ratio of 5×10^{-7} . The solid curve shows the best fit.

We examine the probability to obtain this result and evaluate the 90% CL upper limit using a toy MC simulation. The toy MC generates signal and BG events according to their PDFs fixing the expected number of BG events (\tilde{b}) at $\tilde{b} = b$, while varying the number of signal events (\tilde{s}). For every assumed \tilde{s} , 10,000 samples are generated following Poisson statistics with means \tilde{s} and \tilde{b} for the signal and BG, respectively; the signal yield (s^{MC}) is evaluated by the UEML fit. To obtain the upper limit at the 90% CL (\tilde{s}_{90}) we take an \tilde{s} value that gives a 10% probability for s^{MC} to be smaller than s . The probability to obtain $s \leq -3.9$ is 25% in the case of a null true signal. In other words, due to BG fluctuations a negative s value is possible with a large probability, although the physical signal rate is positive [21].

The toy MC provides an upper limit on the signal at the 90% CL as $\tilde{s}_{90} = 2.0$ events from the UEML fit. We then obtain the upper limit on the branching ratio $\mathcal{B}_{90}(\tau \rightarrow \mu\gamma)$ at the 90% CL as

$$\mathcal{B}_{90}(\tau^- \rightarrow \mu^- \gamma) \equiv \frac{\tilde{s}_{90}}{2\epsilon N_{\tau\tau}} = 4.1 \times 10^{-8}, \quad (2)$$

where the number of τ pairs produced is $N_{\tau\tau} = (4.77 \pm 0.07) \times 10^8$, and the detection efficiency for the 2σ ellipse region is $\epsilon = 5.07\%$.

The systematic uncertainties for the BG PDF shape increase \tilde{s}_{90} to 2.2 [22].

The other systematic uncertainties arise from the track reconstruction efficiency (2.0%), the photon reconstruction efficiency (2.0%), the selection criteria (2.2%), the luminosity (1.4%), the trigger efficiency (0.9%), and the MC statistics (0.3%). All contributions are added in quadrature to obtain the total uncertainty of 4.0%. This uncertainty increases the upper limit on the branching ratio by 0.2% [22]. Since the angular distribution for $\tau \rightarrow \mu\gamma$ depends on the LFV interaction structure, we evaluate its effect on the result by assuming the maximum possible variation, $V \pm A$ interactions, rather than the uniform distribution that is the default in the MC analysis. No appreciable effect is found for the upper limit.

Finally, the following upper limit on the branching ratio is obtained:

$$\mathcal{B}(\tau^- \rightarrow \mu^- \gamma) < 4.5 \times 10^{-8} \quad \text{at the 90\% CL.} \quad (3)$$

3 $\tau \rightarrow e\gamma$

For $\tau \rightarrow e\gamma$ we use a procedure similar to that for $\tau \rightarrow \mu\gamma$.

3.1 Event Selection

We examine a $\tau^+\tau^-$ sample, in which one τ decays to an electron and a photon, and the other τ decays to a charged particle, but not an electron (e), neutrino(s) and any number of photons. Because the selection criteria are quite similar to those for $\tau \rightarrow \mu\gamma$, below we describe only the differences.

An obvious difference is the replacement of the μ by an e on the signal side, and using an e veto (e) rather than a μ veto (μ) on the tag side. The electron on the signal side ($e\gamma$) is required to have $\mathcal{L}_e > 0.90$ and a momentum $p > 1.0$ GeV/ c , while the e on the tag side should have $\mathcal{L}_e < 0.1$. Minor differences in the kinematical selection include requirements on the missing mass squared on the tag side and the opening angle between the tag-side track and the missing particle on the tag side: $-0.5 \text{ GeV}^2/c^4 < m_\nu^2 < 2.0 \text{ GeV}^2/c^4$, and $0.4 < \cos\theta_{\text{miss}-e}^{\text{CM}} < 0.99$. The other requirements are the same as those for $\tau \rightarrow \mu\gamma$, as shown in Fig. 4.

The M_{inv} and ΔE resolutions are $\sigma_{M_{\text{inv}}}^{\text{high/low}} = 14.76 \pm 0.18 / 25.38 \pm 0.38$ MeV/ c^2 and $\sigma_{\Delta E}^{\text{high/low}} = 35.66 \pm 0.62 / 89.98 \pm 1.72$ MeV. The 5σ region with $1.65 \text{ GeV}/c^2 < M_{\text{inv}} < 1.85 \text{ GeV}/c^2$ and $-0.45 \text{ GeV} < \Delta E < 0.18 \text{ GeV}$ is used for the signal evaluation. A 3σ ellipse is also blinded.

After the selection requirements we find 42 and 34.7 ± 3.3 events outside the blind in the 5σ region in data and MC, respectively. As our MC study shows, the BG comes from $\tau^+\tau^-\gamma$ events.

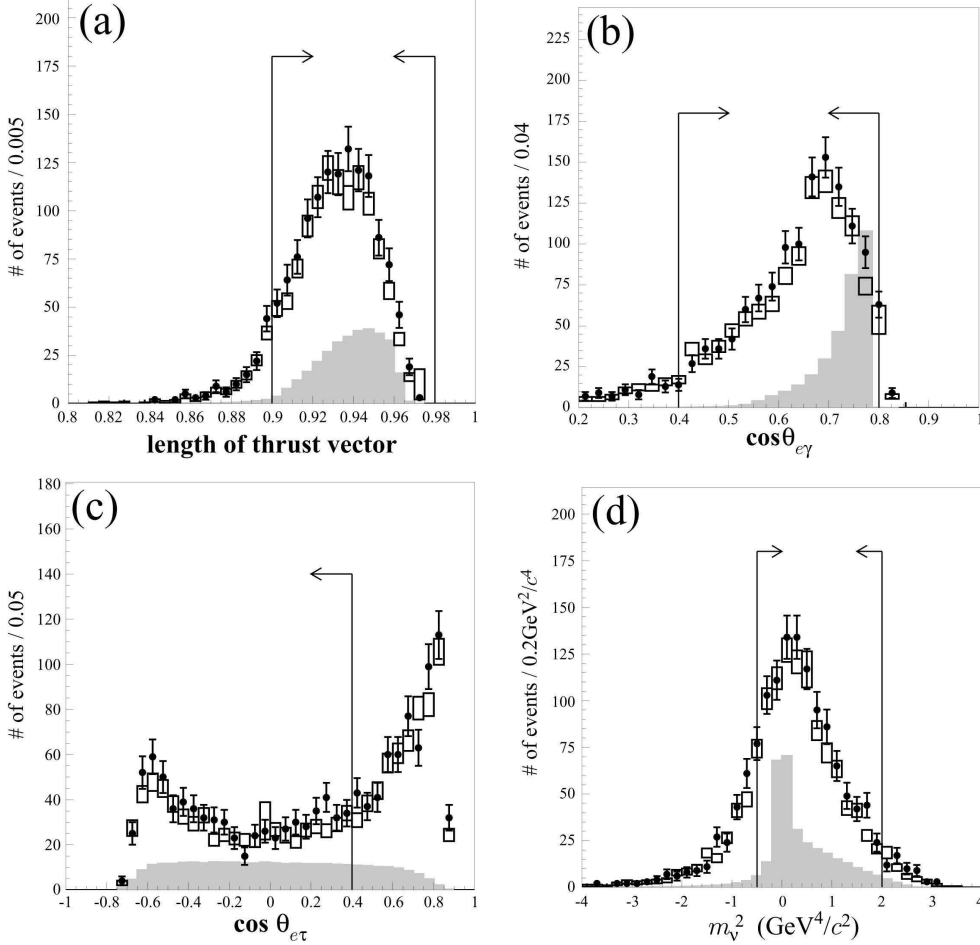


Fig. 4. (a) Magnitude of the thrust vector, (b) $\cos\theta_{e\gamma}^{\text{CM}}$, (c) $\cos\theta_{e\tau}$ and (d) m_{ν}^2 distributions for $\tau \rightarrow e\gamma$. Dots are data, open boxes show the BG Monte Carlo(MC) distribution and shaded histograms are the signal MC. Arrows indicate the selected region. Here, the branching ratio of $\tau \rightarrow e\gamma$ is assumed to be 5.0×10^{-6} for the signal MC histograms. The requirements on particle identification for the signal and tag sides and $1.5 \text{ GeV}/c^2 < M_{\text{inv}} < 2.0 \text{ GeV}/c^2$, $-0.5 \text{ GeV} < \Delta E < 0.5 \text{ GeV}$ were applied for these figures.

3.2 Signal extraction

After opening the blind we find 13 and 55 data events in the blinded region and 5σ region, respectively, while the MC predicts 8.1 ± 1.6 and 42.8 ± 3.7 events, respectively. Figure 5(a) shows the event distribution in the $M_{\text{inv}}-\Delta E$ plane.

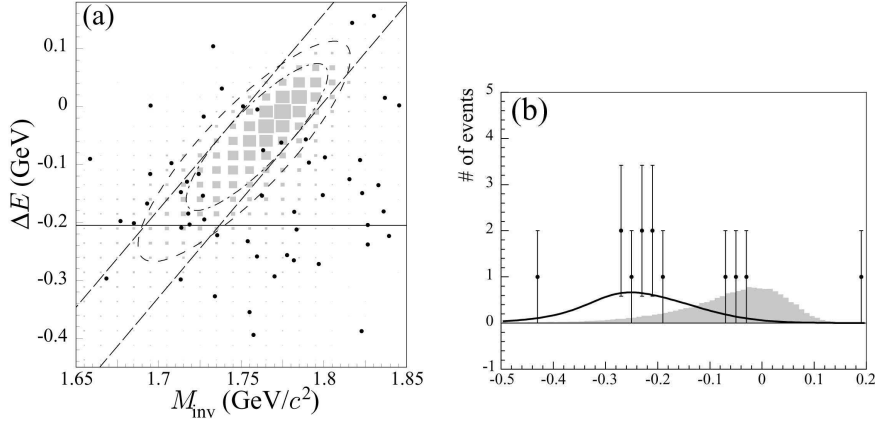


Fig. 5. (a) $M_{\text{inv}} - \Delta E$ distribution in the search for $\tau \rightarrow e\gamma$ in the 5σ region. Dots are the data and shaded boxes indicate the signal MC. The dashed ellipse shows the 3σ blinded region and the dot-dashed ellipse is the 2σ signal region. The dashed lines indicate the 2σ band of the shorter ellipse axis, projected onto the longer ellipse axis. The solid line indicates the dense BG region. (b) Data distribution within the 2σ band. Here, $\mathcal{E} \equiv \Delta E - \Delta E^{(0)}$, $\mathcal{M} \equiv 3.0 \times c^2 \times (M_{\text{inv}} - M_{\text{inv}}^{(0)})$ and $\alpha = 48^\circ$. We obtain the most probable values $\Delta E^{(0)}$ and $M_{\text{inv}}^{(0)}$, $M_{\text{inv}}^{(0)} = 1.775 \text{ GeV}/c^2$, $\Delta E^{(0)} = -2 \text{ MeV}$, by a fit of the signal MC distribution to an asymmetric Gaussian. Points with error bars are the data and the shaded histogram is the signal MC assuming a branching ratio of 5×10^{-7} . The solid curve shows the best fit.

The signal extraction process is the same as that for $\tau \rightarrow \mu\gamma$, described in the former section. The BG is composed of $(18 \pm 18)\%$ $e^+e^-\gamma$ (radiative Bhabha), while the remainder is $\tau^+\tau^-\gamma$. No other background source is found in MC. The UEML fit over the 2σ ellipse region results in $s = -0.14^{+2.18}_{-2.45}$, $b = 5.14^{+3.86}_{-2.81}$ with $N = 5$. The toy MC gives a probability of 48% to obtain $s \leq -0.14$ in the case of a null signal. Figure 5(b) is the same as Fig. 3(b), but for the $\tau \rightarrow e\gamma$ case. The upper limit of $\tilde{s}_{90} = 3.3$ is obtained by the toy MC in the case of the UEML fit result. The upper limit on the branching ratio is calculated as

$$\mathcal{B}_{90}(\tau^- \rightarrow e^-\gamma) \equiv \frac{\tilde{s}_{90}}{2\epsilon N_{\tau\tau}} = 11.7 \times 10^{-8}, \quad (4)$$

where the detection efficiency for the 2σ ellipse region is $\epsilon = 2.99\%$.

The systematic uncertainties for the BG PDF shape increase \tilde{s}_{90} to 3.4. The other systematic uncertainties are similar to those for $\tau \rightarrow \mu\gamma$; minor differences are in the selection criteria (2.5%) and the trigger efficiency (2.0%). The total uncertainty is 4.5%, and it increases the upper limit on the branching ratio by 0.2%. Taking into account this systematic error, we obtain the 90% CL upper limit,

$$\mathcal{B}(\tau^- \rightarrow e^-\gamma) < 12.0 \times 10^{-8}. \quad (5)$$

4 Summary

We have updated our searches for the LFV decay modes, $\tau \rightarrow \mu\gamma$ and $\tau \rightarrow e\gamma$, using 535 fb^{-1} of data, corresponding to about six times higher statistics than in the previous publication [13, 14]. In this study, we have introduced four new requirements for $E_{\text{total}}^{\text{CM}}$, m_{ν}^2 , $\cos\theta_{\mu\tau}$ and the magnitude of the thrust vector in the $\tau \rightarrow \mu\gamma$ search and three new requirements for m_{ν}^2 , $\cos\theta_{e\tau}$ and the magnitude of the thrust vector in the $\tau \rightarrow e\gamma$ search. As a result of the optimized selection criteria, we obtain $\epsilon = 5.07$ (2.99)% and $N_{\text{obs}} = 10$ (5) events in the 2σ elliptical signal region for $\tau \rightarrow \mu\gamma$ ($e\gamma$) in this analysis, compared to $\epsilon = 12.0$ (6.39)% and $N_{\text{obs}} = 54$ (20) events over a 5σ signal box in our previous study. The improved selection leads to a value of $\epsilon/\sqrt{N_{\text{obs}}}$ that is almost the same as that in the previous analysis, and therefore the expected upper limit, which is approximately proportional to $\sqrt{N_{\text{obs}}}/(\epsilon \int Ldt)$ in the case of no signal, has improved as $1/\int Ldt$ rather than in proportion to $1/\sqrt{\int Ldt}$, as would be the case if the previous selection criteria were used. (Here $\int Ldt$ is the integrated luminosity.)

The resulting upper limits on the branching ratios are

$$\mathcal{B}(\tau^- \rightarrow \mu^- \gamma) < 4.5 \times 10^{-8}, \quad (6)$$

$$\mathcal{B}(\tau^- \rightarrow e^- \gamma) < 12.0 \times 10^{-8} \quad (7)$$

at the 90% CL.

The limit on the branching ratio of the $\tau^- \rightarrow \mu^- \gamma$ decay is the most stringent among all LFV decays of the τ lepton to date. Our results constrain the parameter space of various theoretical models that predict LFV decays [1–3].

Acknowledgments

We thank the KEKB group for the excellent operation of the accelerator, the KEK cryogenics group for the efficient operation of the solenoid, and the KEK computer group and the National Institute of Informatics for valuable computing and Super-SINET network support. We acknowledge support from the Ministry of Education, Culture, Sports, Science, and Technology of Japan and the Japan Society for the Promotion of Science; the Australian Research Council and the Australian Department of Education, Science and Training; the National Science Foundation of China and the Knowledge Innovation Program of the Chinese Academy of Sciences under contract No. 10575109 and

IHEP-U-503; the Department of Science and Technology of India; the BK21 program of the Ministry of Education of Korea, and the CHEP SRC program and Basic Research program (grant No. R01-2005-000-10089-0) of the Korea Science and Engineering Foundation; the Polish State Committee for Scientific Research under contract No. 2P03B 01324; the Ministry of Science and Technology of the Russian Federation; the Slovenian Research Agency; the Swiss National Science Foundation; the National Science Council and the Ministry of Education of Taiwan; and the U.S. Department of Energy.

References

- [1] A. Brignole and A. Rossi, Nucl. Phys. B **701**, 3 (2004).
- [2] L. Calibbi, A. Faccia, A. Masiero and S.K. Vempati, Phys. Rev. D **74**, 116002 (2006).
- [3] J.R. Ellis, J. Hisano, M. Raidal and Y. Shimizu, Phys. Rev. D **66**, 115013 (2002).
- [4] K. G. Hayes *et al.* (MARK-II Collaboration), Phys. Rev. D **25**, 2869 (1982).
- [5] S. Keh *et al.* (Crystal Ball Collaboration), Phys. Lett. B **212**, 123 (1988).
- [6] H. Albrecht *et al.* (ARGUS Collaboration), Z. Phys. C **55**, 179 (1992).
- [7] A. Bean *et al.* (CLEO Collaboration), Phys. Rev. Lett. **70**, 138 (1993).
- [8] P. Abreu *et al.* (DELPHI Collaboration), Phys. Lett. B **359**, 411 (1995).
- [9] K. W. Edwards *et al.* (CLEO Collaboration), Phys. Rev. D **55**, R3919 (1997).
- [10] S. Ahmed *et al.* (CLEO Collaboration), Phys. Rev. D **61**, 071101 (2000).
- [11] A. Abashian *et al.* (Belle Collaboration), Nucl. Instr. Meth. A **479**, 117 (2002).
- [12] S. Kurokawa and E. Kikutani, Nucl. Instr. Meth. A **499**, 1 (2003), and other papers included in this Volume.
- [13] K. Abe *et al.* (Belle Collaboration), Phys. Rev. Lett. **92**, 171802 (2004).
- [14] K. Hayasaka *et al.* (Belle Collaboration), Phys. Lett. B **613**, 20 (2005).
- [15] B. Aubert *et al.* (BaBar Collaboration), Phys. Rev. Lett. **95**, 041802 (2005).
- [16] B. Aubert *et al.* (BaBar Collaboration), Phys. Rev. Lett. **96**, 041801 (2006).
- [17] S. Jadach, B. F. L. Ward and Z. Wąs, Comput. Phys. Commun. **130**, 260 (2000).
- [18] CERN Program Library Long Writeup No. W5013 1993.
- [19] A. Abashian *et al.*, Nucl. Instr. Meth. A **491**, 69 (2002).

- [20] K. Hanagaki *et al.*, Nucl. Instr. Meth. A **485**, 490 (2002).
- [21] We restricted s to be positive in the previous analysis. Due to BG fluctuations, however, s can be negative as we found in this case. Our previous upper limit is then reduced by a factor of $\simeq 3$ when negative s is allowed.
- [22] A method to incorporate the systematic uncertainties into a branching ratio is discussed in Ref. [10].